

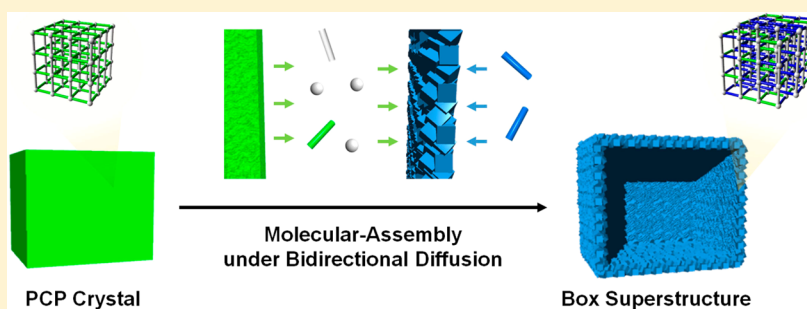
# Diffusion-Coupled Molecular Assembly: Structuring of Coordination Polymers Across Multiple Length Scales

Kenji Hirai,<sup>†</sup> Julien Reboul,<sup>‡</sup> Nobuhiro Morone,<sup>‡</sup> John E. Heuser,<sup>‡</sup> Shuhei Furukawa,<sup>\*,‡</sup> and Susumu Kitagawa<sup>\*,†,‡</sup>

<sup>†</sup>Department of Synthetic Chemistry and Biological Chemistry, Graduate School of Engineering, Kyoto University, Katsura, Nishikyo-ku, Kyoto 615-8510, Japan

<sup>‡</sup>Institute for Integrated Cell-Material Science (WPI-iCeMS), Kyoto University, Yoshida, Sakyo-ku, Kyoto 606-8501, Japan

**S** Supporting Information



**ABSTRACT:** Porous coordination polymers (PCPs) are an intriguing class of molecular-based materials because of the designability of framework scaffolds, pore sizes and pore surface functionalities. Besides the structural designability at the molecular scale, the structuring of PCPs into mesoscopic/macroscopic morphologies has attracted much attention due to the significance for the practical applications. The structuring of PCPs at the mesoscopic/macroscopic scale has been so far demonstrated by the spatial localization of coordination reactions on the surface of templates or at the phase boundaries. However, these methodologies have never been applied to the fabrication of solid-solution or multivariate metal–organic frameworks (MOFs), in which multiple components are homogeneously mixed. Herein, we demonstrate the structuring of a box-type superstructure comprising of a solid-solution PCP by integrating a bidirectional diffusion of multiple organic ligands into molecular assembly. The parent crystals of  $[\text{Zn}_2(\text{ndc})_2(\text{bpy})]_n$  were placed in the DMF solution of additional organic component of  $\text{H}_2\text{bdc}$ , and the temperature was rapidly elevated up to  $80^\circ\text{C}$  ( $\text{ndc}$  = 1,4-naphthalenedicarboxylate,  $\text{bpy}$  = 4,4'-bipyridyl,  $\text{bdc}$  = 1,4-benzenedicarboxylate). The dissolution of the parent crystals induced the outward diffusion of components; contrariwise, the accumulation of the other organic ligand of  $\text{H}_2\text{bdc}$  induced the inward diffusion toward the surface of the parent crystals. This bidirectional diffusion of multiple components spatially localized the recrystallization at the surface of cuboid parent crystals; therefore, the nanocrystals of a solid-solution PCP ( $[\text{Zn}_2(\text{bdc})_{1.5}(\text{ndc})_{0.5}(\text{bpy})]_n$ ) were organized into a mesoscopic box superstructure. Furthermore, we demonstrated that the box superstructures enhanced the mass transfer kinetics for the separation of hydrocarbons.

## INTRODUCTION

Molecular assembly provides a facile means to organize a vast number of molecular components into a complex structure.<sup>1–3</sup> This spontaneous organization is accomplished by the weak forces between the components, including hydrogen bond,<sup>4</sup> coordination bond,<sup>5</sup> electrostatic interactions and van der Waals forces.<sup>6</sup> Because these forces act between the adjacent molecules only within a few angstroms, the structural complexity over the scale of individual components cannot be controlled by conventional molecular assembly. Therefore, an intriguing challenge in molecular assembly is how to generate the structural complexity beyond the molecular scale.

One way to create the structural complexities beyond the molecular scale is to carry out the chemical reaction under the controlled diffusion.<sup>7</sup> The diffusion of the reactants localizes the

spatial location of chemical reaction, thus leading to the fabrication of the macroscopic morphologies. As diffusion is simply driven by concentration gradients, the concept of diffusion-coupled reaction is applicable to molecular assembly. The structural complexities in the molecular scale can be precisely controlled by molecular assembly so that the diffusion-coupled molecular assembly will be a new strategy to control the structural complexities from molecular to mesoscopic/macroscopic scales.

The assembly of organic ligands with metal ions via coordination bonds gives porous extended frameworks, so-called porous coordination polymers (PCPs) or metal–organic

Received: August 4, 2014

Published: September 25, 2014

frameworks (MOFs).<sup>8,9</sup> A judicious choice of metal ions and organic ligands allows the design of framework scaffolds, pore shapes and pore surface functionalities.<sup>10</sup> The designability of PCPs enables one to control the interaction between the pores and guest species, thus presenting PCPs/MOFs as a new class of porous materials for gas storage,<sup>11</sup> gas separation<sup>12</sup> and heterogeneous catalysis.<sup>13</sup> A strategy for further improving the porous properties is to introduce complexity in a framework by increasing the number of components. Multiple organic ligands with distinct chemical functionality can be intermingled within a single framework, i.e., solid-solution PCP or multivariate MOF,<sup>14</sup> which significantly enhances the selectivity of gas adsorption. As stated above, the structural complexities of PCPs in the molecular scale are rationally controlled by the conventional molecular assembly.

On the other hand, considerable effort has been devoted to structuring of PCPs in the mesoscopic/macroscale,<sup>15</sup> e.g., thin films,<sup>16</sup> patterns,<sup>17</sup> hollow spheres,<sup>18</sup> and core-shell particles,<sup>19</sup> due to the significance of the morphologies for the practical applications. A key for structuring of PCPs is to localize coordination reactions at a desired position. The localization of coordination reaction has been traditionally achieved on the substrate by the induction of heterogeneous nucleation.<sup>20</sup> Most recently, the reactions at the phase boundaries (liquid/solid<sup>17b,21</sup> and liquid/liquid<sup>18a,22</sup> interfaces) have attracted much attention because of the high capability of spatial localization of coordination reactions. To date, however, these methodologies have been limited to the single phase PCPs that can be synthesized under a wide range of reaction conditions. In other words, the general method for structuring the solid-solution PCP has not been established yet.

Our strategy to build structural complexities in PCPs from molecular to mesoscopic/macroscale is to carry out the molecular assembly under a bidirectional diffusion of two organic ligands with a same coordinating group. Herein, we demonstrate the fabrication of a box superstructure of solid-solution PCP. The cuboid parent crystals of  $[\text{Zn}_2(\text{ndc})_2(\text{bpy})]_n$  are heated in the solution of  $\text{H}_2\text{bdc}$  ( $\text{ndc} = 1,4\text{-naphthalenedicarboxylate}$ ,  $\text{bpy} = 4,4'\text{-bipyridyl}$ ,  $\text{bdc} = 1,4\text{-benzenedicarboxylate}$ ). The dissolution of the parent crystal induces the outward diffusion of  $\text{Zn}^{2+}$ ,  $\text{ndc}$  and  $\text{bpy}$ ; contrariwise, the recrystallization induces inward diffusion of  $\text{bdc}$  toward the surface of the parent crystals. Consequently, all components ( $\text{Zn}^{2+}$ ,  $\text{ndc}$ ,  $\text{bpy}$  and  $\text{bdc}$ ) are recrystallized at the surface of parent crystals, leading to the formation of a hollow box superstructure of the solid-solution PCP of  $[\text{Zn}_2(\text{bdc})_{1.5}(\text{ndc})_{0.5}(\text{bpy})]_n$  (Figure 1). The resulting solid-solution PCP is doubly interpenetrated, which improves the sorption amount by stabilizing the evacuated phase. By taking

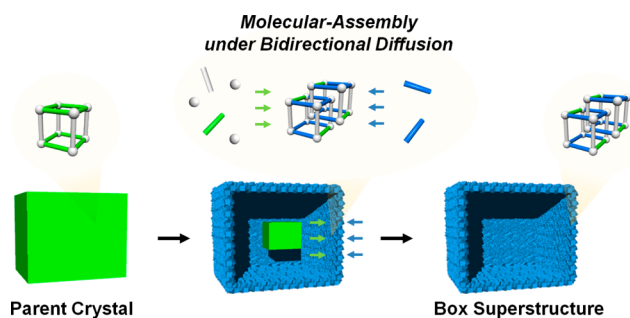


**Figure 1.** Molecular assembly under the bidirectional diffusion: fabrication of a box superstructure of a solid-solution PCP.

an advantage of the resulting hollow-structured materials, in which the internal void improves the mass transfer kinetics of molecules, we demonstrate that the box superstructure shortens the separation time of hydrocarbons.

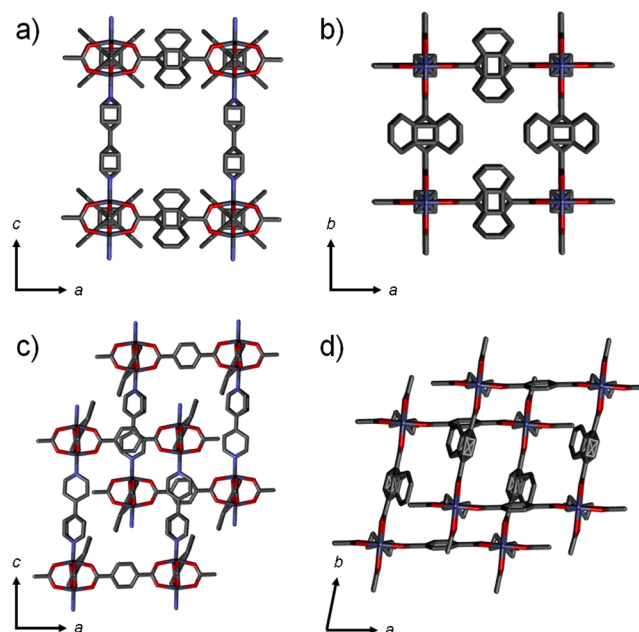


**Figure 2.** Crystal structure of as-synthesized 1: (a) the view from  $b$  axis, and (b) the view from  $c$  axis. The crystal structure of as-synthesized 2: (c) the view from dicarboxylate direction, and (d) the view from  $\text{bpy}$  direction.

## RESULTS AND DISCUSSION

**Emergence of Structural Complexities across Multiple Length Scales.** We chose a series of three-dimensional frameworks,  $[\text{M}_2\text{L}_2\text{P}]_n$  ( $\text{M}$ : divalent metal ion,  $\text{L}$ : dicarboxylate layer ligand,  $\text{P}$ : dipyriddy pillar ligand),<sup>23</sup> in which the dicarboxylate layer ligands link to the dimetal paddlewheel clusters to form two-dimensional square lattices connected by dipyriddy pillar ligands at the lattice points. This series of frameworks is an excellent candidate to demonstrate the structuring of a solid-solution PCP, because the multiple organic ligands can be intermingled within a framework.<sup>24</sup> The reaction of PCP crystals of  $[\text{M}_2\text{L}_2\text{P}]_n$  with another dicarboxylate was carried out for generating the bidirectional flow (one direction: dissolution of parent crystals; counter direction: accumulation of the other organic ligand toward the surface of parent crystals).

The microcrystals of  $[\text{Zn}_2(\text{ndc})_2(\text{bpy})]_n$  (**1**) were synthesized by microwave reaction (Figure 3a). The dozens of microcrystals of **1** were placed in DMF solution of  $\text{H}_2\text{bdc}$ , and the temperature was rapidly elevated and kept at  $80^\circ\text{C}$  for 30 min by a microwave reactor (DMF =  $N,N$ -dimethylformamide). After cooling and drying, the cuboid particles, whose sizes were nearly same as the original cuboid crystals of **1** ( $5 \times 5 \times 10 \mu\text{m}^3$ ), were observed by scanning electron microscope (SEM) (Figure 3b). The SEM image with a higher magnification showed that the nanocrystals ( $\sim 200$  nm) were assembled to form a cuboid superstructure (Figure 3c). To elucidate the three-dimensional macroscopic structure, the dried cuboid superstructure embedded into a thermoset epoxy resin was solidified and sliced by an ultramicrotome. The ultrathin section of cuboid superstructure was observed by transmission electron microscope (TEM). As

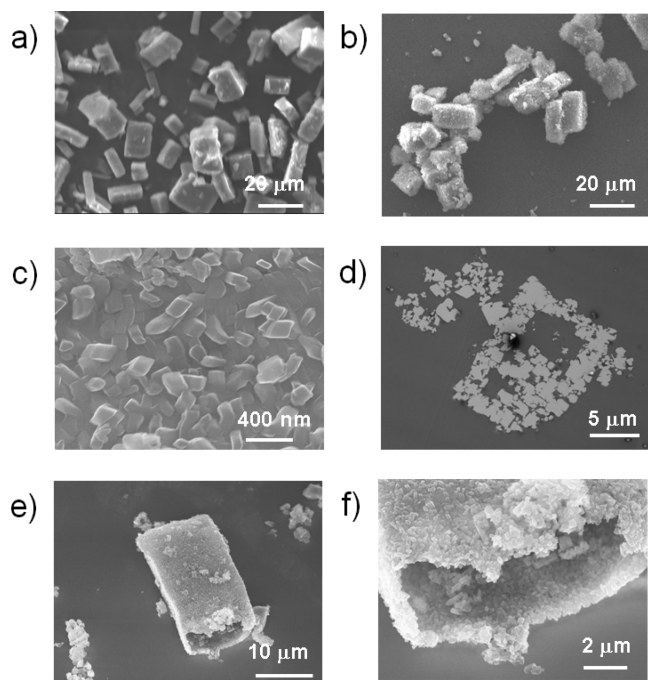


**Figure 3.** (a) SEM image of the parent crystals of **1**, (b) SEM image of the box superstructures, (c) SEM image of the side wall of the box superstructure at a high magnification. The nanocrystals are aggregated to form the wall of box superstructure. (d) TEM image of the ultrathin section of the box superstructure. The void is observed in the square-shaped assemblage of nanocrystals. (e,f) SEM image of the box superstructure after ultrasonication. The internal void is observed from the broken edge of the box superstructure.

shown in Figure 3d, the internal void was seen in the cross-section of the cuboid superstructure. To further analyze the three-dimensional macroscopic structure, the cuboid superstructure was partially broken by ultrasonication. The interior void of the cuboid superstructure was clearly observed after breaking the edge of the box superstructure (Figure 3e,f). These results suggested that the cuboid crystals of **1** were converted to the box superstructures.

Powder X-ray diffraction (PXRD) measurements were carried out to determine the framework structure of the box superstructure. As shown in Figure S1 (Supporting Information), the XRD pattern of the box superstructure nearly corresponds to that of **1**, suggesting that the box superstructure possesses the framework structure analogous to  $[M_2L_2P]_n$ . Furthermore, in order to elucidate the chemical compositions of the box superstructure, the  $^1\text{H}$  NMR experiments were carried out for the solution prepared by the digestion of box superstructure with hydrochloric acid. The ratio of dicarboxylates (bdc and ndc) to bpy was estimated to be 2:1, corresponding to the chemical composition of  $[M_2L_2P]_n$ . The ratio of bdc and ndc in the box superstructure was estimated to be 3:1, which means that pure phase of **1** was converted to a solid-solution PCP,  $[\text{Zn}_2(\text{bdc})_{1.5}(\text{ndc})_{0.5}(\text{bpy})]_n$  (**2**) (Figure S2). These results indicated that the dissolution of parent crystal of **1** and the simultaneous recrystallization of **2** led to the formation of the box superstructure.

In order to clarify the crystal structure of solid-solution PCP of  $[\text{Zn}_2(\text{bdc})_{1.5}(\text{ndc})_{0.5}(\text{bpy})]_n$  (**2**), we synthesized the single crystal of **2** by the following procedure. The methanol solution of bpy, the buffer solution of DMF/methanol mixture, and the DMF solution of  $\text{Zn}(\text{NO}_3)_2 \cdot 6\text{H}_2\text{O}$ ,  $\text{H}_2\text{bdc}$  and  $\text{H}_2\text{ndc}$  were

layered sequentially from bottom to top in a narrow glass tube. The glass tube was kept at  $90^\circ\text{C}$  for 2 days and the single crystals of **2** with the size of  $10\ \mu\text{m}$  were harvested. The crystal structure of as-synthesized **2** was successfully determined by a single crystal X-ray diffraction analysis (Figure 2c,d). As in the case of the crystal structure of **1**, the dicarboxylates bridge the zinc paddlewheel clusters to form two-dimensional square grids linked by bpy at the lattice points. Because the dicarboxylates along *a* axis is close to the upper pyridyl ring of bpy, nonbulky bdc is selectively located therein. In contrast, bdc and ndc were disordered in the position of dicarboxylates along *b* axis at the ratio of 1:1. Therefore, the total ratio of bdc and ndc is calculated to be 3:1, corresponding to the chemical formula of  $[\text{Zn}_2(\text{bdc})_{1.5}(\text{ndc})_{0.5}(\text{bpy})]_n$  determined by  $^1\text{H}$  NMR. The partial replacement from ndc to nonbulky bdc generates a space in the framework to accommodate another framework therein; thus the two frameworks are doubly interpenetrated in **2**. The simulated XRD pattern of **2** corresponds to the PXRD pattern of the box superstructure, indicating that the box superstructure consists of solid-solution type PCP of **2** (Figure S1c,d).

#### Mechanism of Diffusion-Coupled Molecular Assembly.

In order to investigate the formation mechanism of box morphology of the solid-solution PCP (**2**) under the bidirectional diffusion, we carried out a series of synthetic experiments, in which the reaction time was systematically varied (10 s to 30 min) and the resulting structure was analyzed by PXRD measurements. As shown in Figure S3, the PXRD patterns were identical throughout the reaction, suggesting that the framework structure of  $[M_2L_2P]_n$  was maintained. After the digestion of the resulting compounds by hydrochloric acid, the chemical compositions were analyzed by the  $^1\text{H}$  NMR experiments. (Figures 4a and S4–S17). As shown in Figure 4a, the ratio of bdc to (bdc and ndc) reached 0.75 (bdc:ndc = 3:1) within 4 min, corresponding to the chemical formula of  $[\text{Zn}_2(\text{bdc})_{1.5}(\text{ndc})_{0.5}(\text{bpy})]_n$  (**2**). This ratio of bdc to (bdc and ndc) did not change even after the extension of the reaction time to 30 min.

In addition to the analyses of the resulting framework, the residual reaction solution was analyzed by the  $^1\text{H}$  NMR experiments (Figures 4b and S18–S23, and Table S1). To evaluate the molar amounts of bdc and ndc, 0.1 mmol of methanol was added in the NMR sample solution as an external reference. The molar amounts of bdc and ndc were estimated by comparing the integration areas of bdc and ndc with that of methanol. The migration amounts of bdc and ndc were calculated by the subtraction of molar amount at a certain reaction time from the original molar amount. Figure 4b showed the migration amounts of inward bdc and outward ndc versus time, which suggests that the larger amount of ndc was eluted (parent crystal of **1**  $\rightarrow$  solution) than the amount of bdc for the crystallization (solution  $\rightarrow$  crystal of **2**). As a consequence, less amount of dicarboxylates (bdc and ndc) was consumed in the recrystallization of **2** than the elution of dicarboxylates into the solution. The amount of dicarboxylates in solid decreased by 33 mol % at 4 min (Table S1), resulting in the reduction of the total amount of crystals. In addition to the difference in migration amounts of ndc and bdc, the framework interpenetration in **2** also decreased the crystal volume by 20% (the density of **1**:  $1.148\ \text{g cm}^{-3}$ , the density of **2**:  $1.434\ \text{g cm}^{-3}$ ). The decreases of the volume and the amount of crystals leads to the formation of the void inside the cuboid structure, thus giving rise to the box superstructure.

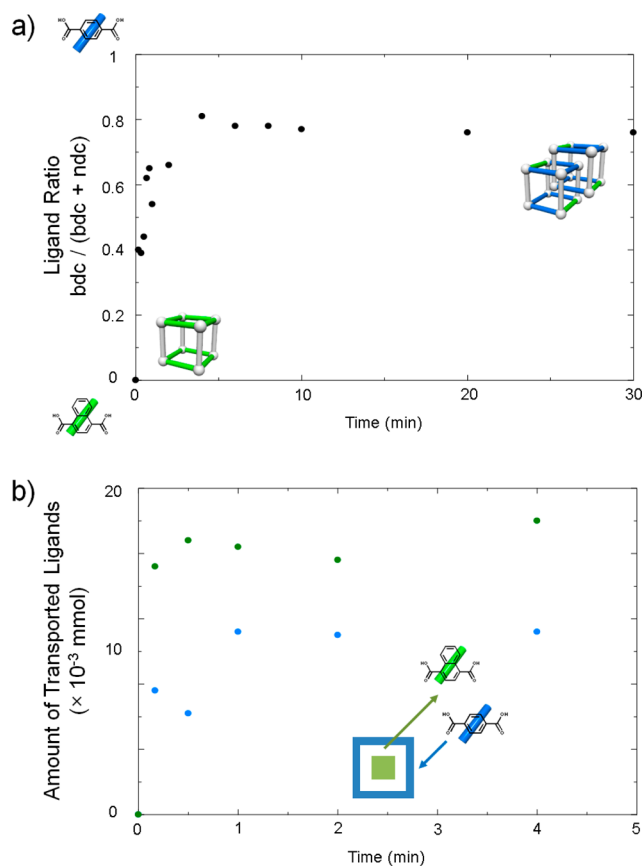


**Figure 4.** Chronological change of (a) the ratio of bdc and ndc in the solid-state compounds, (b) transported amount of bdc (blue) and ndc (green).

The formation of a box superstructure was similarly observed in the single crystal of **1** in the millimeter scale. Prior to carrying out diffusion-coupled molecular assembly, a single crystal of **1** ( $2 \times 2 \times 1 \text{ mm}^3$ ) was synthesized by hydrothermal reaction (Figure S4a). The single crystal of **1** was placed in a DMF solution of  $\text{Zn}_2(\text{NO}_3)_2 \cdot 6\text{H}_2\text{O}$ ,  $\text{H}_2\text{bdc}$ , bpy, and the solution was kept at  $120^\circ\text{C}$  for 2 days by an oil-bath heater. After the reaction, a cuboid

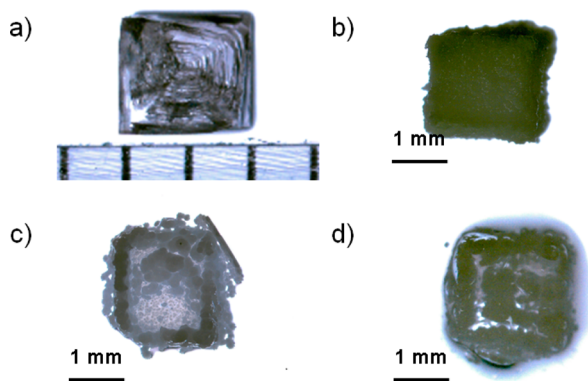


**Figure 5.** Optical microscopic images of (a) the millimeter-sized parent crystal, (b) the box superstructure, (c) the box superstructure whose upper surface was removed by a knife, (d) the intermediate of the box superstructure whose upper surface was removed by a knife (the reaction stops at 1 day). The portion of the parent crystal is still remained in the box.

particle, whose size was same as the original single crystal of **1**, was observed by optical microscope (Figure 5b). To see the internal void, the upper surface of cuboid particle was manually sliced with a knife. The internal void was clearly seen by an optical microscope as shown in Figure 5c, indicating that the cuboid crystal was converted to a box superstructure of **2**. To unveil the conversion process from the cuboid crystal to the box superstructure, the reaction was stopped at 1 day and the upper surface of the obtained cuboid particle was sliced. A portion of the original crystal of **1** was still remained in the internal void, i.e., yolk-shell structure, as shown in Figure 5d. These results indicate that the box superstructure was formed via the yolk-shell structure.

When a millimeter-sized crystal of **1** was heated in the solution of only  $\text{H}_2\text{bdc}$  by an oil-bath heater, the parent crystal of **1** was converted into the microcrystalline powders without keeping the cuboid morphology (Figure S25). The difference between the reactions of microcrystals and millimeter-sized crystal can be explained as follows. The rapid heating by microwave reactor induces faster recrystallization of **2** than the oil-bath heating,<sup>17b</sup> and enables to localize the recrystallization nearby the surface of parent crystal and to maintain the cuboid morphology. While the microwave reaction gave the box superstructures for the microcrystals as shown above, it was not applicable to the millimeter-sized crystal of **1** due to its fragility; the large crystal was mechanically cracked under the abrupt increase of temperature induced by microwave reaction. Therefore, it is required to find the reaction condition accelerating the crystallization under oil-bath heating for the conversion of the millimeter-sized crystal. By optimizing the synthetic conditions, we found that the presence of  $\text{Zn}^{2+}$ , ndc and bpy together with  $\text{H}_2\text{bdc}$  in the initial solution enables to accelerate the crystallization of **2** and slow down the dissolution of **1**, leading to the proper dissolution/recrystallization kinetics for the replication.

Interestingly, the crystals of **2** were grown on the parent crystal of **1** with maintaining the original orientation of **1** along the surface normal direction (Figure S26). Although the in-plane X-ray diffraction was difficult to be carried out because of the rough surface of the box superstructure, the crystals were apparently not oriented in the in-plane direction, as seen in Figure 5b,c. This is most likely because of the lattice mismatch between **1** and **2**; whereas **1** possesses the perfect tetragonal framework ( $\alpha = \beta = \gamma = 90^\circ$ ), **2** consists of two distorted frameworks of  $[\text{M}_2\text{L}_2\text{P}]$  (inner angle between three zinc lattice points:  $79.82^\circ$  on  $ab$  plane and  $86.91^\circ$  on  $ac$  plane). Because of such a distortion from tetragonal symmetry, the crystal of **2** was grown only with the orientation along the surface normal direction,<sup>25</sup> as seen in the growth on substrates functionalized with self-assembled monolayers.<sup>26</sup>

On the basis of these experiments, we propose the reaction process as follows. (1) The cuboid crystals of **1** are dissolved and the components ( $\text{Zn}^{2+}$ , ndc and bpy) are eluted to the solution. (2) The solid-solution PCP of **2** is rapidly crystallized on the surface of **1** by consuming  $\text{Zn}^{2+}$ , ndc and bpy from the parent crystal of **1** and bdc from the starting solution (as shown in Table S2, the elution of  $\text{Zn}^{2+}$  was evidenced by inductively coupled plasma measurement). The coordination geometry and the orientation along the surface normal direction are maintained throughout the crystallization process. (3) The larger amount of ndc was transported from the parent crystal to solution and the smaller amount of bdc was accumulated into the crystal of **2**. The difference of the migration amount of outward ndc and inward bdc reduces the total amount of crystals. In addition, the

interpenetration of frameworks in **2** decreased the volume of crystals. The decreases of amount and volume of crystals generates an internal void in the cuboid structure. Consequently, the box superstructure of solid-solution PCP of **2** is obtained (Figure 6). This reaction mechanism resembles Kirkendall

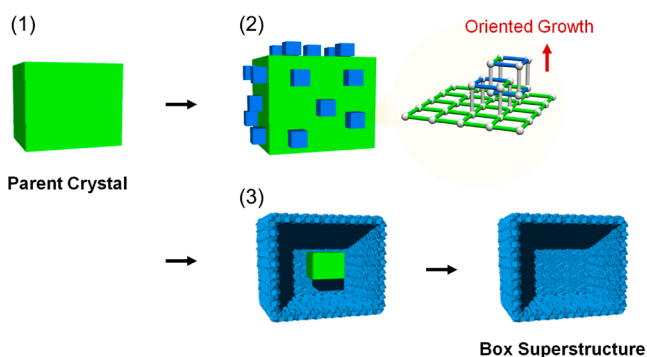


**Figure 6.** Plausible reaction mechanism: (1) The dissolution of parent crystal of **1** provides the components ( $\text{Zn}^{2+}$ , ndc and bpy) in the solution. (2) The solid-solution of **2** is recrystallized on the surface of **1** with keeping the growth orientation along the surface normal direction. (3) The larger amount of ndc eluted than the consumed amount of bdc for the recrystallization of **2** and the formation of interpenetration of **2** decrease the volume of crystals, which leads to the generation of an internal void in the cuboid structure via yolk–shell structure.

effect,<sup>7a,27</sup> in which the internal void is formed because of the unbalanced bidirectional migrations of components; however, the interpenetration of the frameworks also contributes to the formation of interior void in our reaction system. As seen in the hollow structure synthesized by Kirkendall effect,<sup>28</sup> the initial condition, e.g., concentration of  $\text{H}_2\text{bdc}$ , is crucial for the fabrication of the box superstructure (Figure S27).

Since the diffusion is driven by concentration gradients, the diffusion-coupled molecular assembly will be applicable to a various kinds of PCPs or MOFs. Indeed, the formation of a box superstructure was similarly observed in IRMOF analogous structures.<sup>29</sup> The microcrystals of MOF-5 ( $[\text{Zn}_4(\text{O})(\text{bdc})_3]_n$ ) were synthesized at room temperature.<sup>29b</sup> The microcrystals of MOF-5 were placed in a DMF/ethanol solution of  $\text{H}_2\text{abdc}$ , and the solution was kept at 60 °C for 2 h ( $\text{abdc} = 2\text{-aminobenzene-1,4-dicarboxylate}$ ). After the reaction, the box superstructure of solid-solution type MOF  $[\text{Zn}_4(\text{O})(\text{bdc})_{1.8}(\text{abdc})_{1.2}]_n$  was obtained (Figures S28–S30).

**Separation of Hydrocarbons by the Box Superstructure of **2**.** The adsorption measurements of the box superstructure of **2** (denoted as **2-box**) with the size of 5–10  $\mu\text{m}$  were performed for carbon dioxide, nitrogen and oxygen (Figure 7a and Figures S31–S32, respectively). Prior to the adsorption measurements, the sample was evacuated under vacuum at 150 °C. As shown in the single-crystal structure of **2**, the framework was deformed in response to the removal of guest molecules from the pores (Figure S33). The lattice comprising of dicarboxylates and zinc paddlewheels was significantly distorted after the guest removal. The inner angle between three zinc lattice points on the *ab* plane changed from 79.82° to 54.91°. This is because the distortion of the square lattice reduces the void space and stabilizes the evacuated phase. Because of the structural transformation, **2-box** showed the stepwise uptake of carbon dioxide (120 mL/g). In contrast, the powders of **1** adsorbed only small amount of carbon dioxide in spite of the larger void space (40 mL/g) (Figure 7a). The interpenetration of

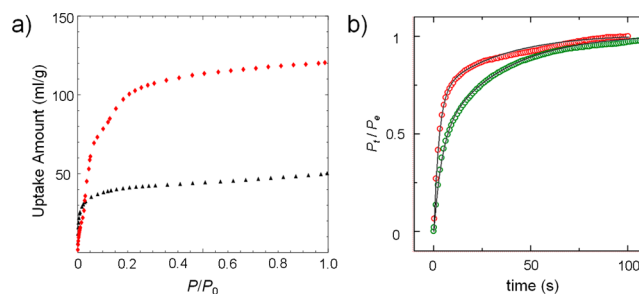


**Figure 7.** (a) Adsorption isotherm of **1** (black) and **2** (red) for carbon dioxide, (b) Adsorption kinetics profiles for carbon dioxide ( $P/P_0 = 0.78$ , 195 K). The sampling rate = 1 s; green: **2-micro** and red: **2-box**, respectively. Corresponding fits for the DE model are also shown as the black line.

frameworks in **2** contributes to the structural stability of evacuated phase (Figure S1e,f); thus, the storage capacity of **2** is much larger than that of **1** with poor crystallinity.<sup>30</sup>

Because **2-box** consists of nanocrystals ( $\sim 200$  nm), we investigated the effect of the crystal size on the sorption properties by comparing **2-box** with the micrometer crystals of **2** (**2-micro**) (5–10  $\mu\text{m}$ ). The adsorption kinetics for carbon dioxide were analyzed by real-time monitoring of the pressure after the introduction of carbon dioxide at  $P/P_0 = 0.78$  into the sample tube. The time dependent uptake ( $P_t/P_e$ ;  $P_t$  is the uptake at time  $t$  and  $P_e$  is the equilibrium uptake) for carbon dioxide on **2-box** and **2-micro** is shown in Figure 7b. The result showed the effect of the crystal size on the kinetics of carbon dioxide uptake; the rate of carbon dioxide sorption for **2-box** is much faster than that for **2-micro**. In order to analyze the sorption kinetics for carbon dioxide depending on the crystal size, we employed the double-exponential (DE) model<sup>31</sup> for the analyses as shown in eq 1,

$$P_t/P_e = A_1\{1 - \exp(-k_1t)\} + A_2\{1 - \exp(-k_2t)\} \quad (1)$$

where  $k_1$  and  $k_2$  are kinetic rate constants, with  $A_1 + A_2 = 1$ . This is because there are two kinetic processes each with different diffusion barriers; one is faster diffusion at the gas/crystal interface and the other is slower diffusion in the pores.<sup>32</sup> Since the diffusions at the crystal surface and in the pores are generally determined by the crystal surface and pore structures, respectively, we applied the global fitting analysis to carbon dioxide sorption kinetics by treating the  $k_1$  and  $k_2$  values as lateral fitting parameters. Kinetic parameters obtained by DE model are summarized in Table S3. The  $A_2$  contribution (pore diffusion in crystals) of **2-micro** for the sorption kinetics of carbon dioxide is significantly larger ( $A_2 = 0.557$ ) than that for **2-box** ( $A_2 = 0.284$ ). It is reasonable to consider that the latter contribution decreases in the case of **2-box**, because the diffusion path is shorter in **2-box** comprising of nanocrystals. Although we employed the single-exponential model that includes only one kinetic rate constant for the analyses, the model did not give a satisfactory fit for the experimental data (Figure S36 and Table S4). The sorption kinetics of **2-box** for hexane was also faster than that of **2-micro** for hexane (Figures S37–S38 and Table S5).

Since **2-box** is an interesting material for separation medium due to the quick adsorption,<sup>33</sup> we investigated the effect of macroscopic superstructure on the separation efficiency. To clarify the effect of the box superstructure, we prepared **2-box** and **2-box** completely decomposed by the ultrasonication, denoted as nanocrystalline powders (**2-NP**) (Figure S39). The narrow glass tubes packed with the two materials (**2-box** and **2-**

NP, respectively) were used for the breakthrough experiments. The procedures to pack the materials into the glass tube (the weight and the process) were identical for each sample. Therefore, the difference in the separation efficiency between **2-box** and **2-NP** in the following section is exclusively explained by their distinct superstructures. The breakthrough experiments were performed for the separation of an equimolar binary mixture of structural isomers, hexane/2,2-dimethylbutane (Figure 8, Figures S40–S42). The PCP of **2** demonstrated a

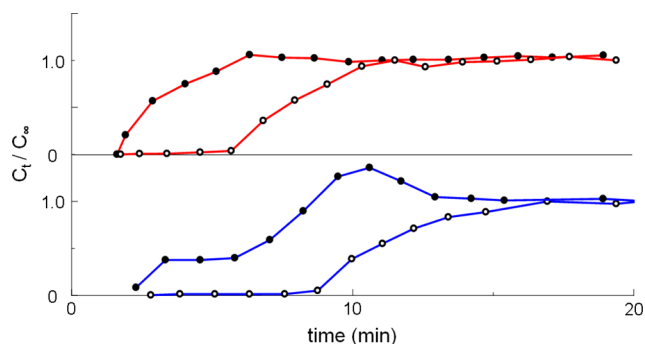


**Figure 8.** Binary breakthrough separation profiles for the equimolar separation of mixture of hexane (open circle)/2,2-dimethylbutane (closed circle) at 25 °C obtained with **2-box** (red) and **2-NP** (blue).

significant hexane/2,2-dimethylbutane separation with a separation selectivity of 2.41 for **2-box** and 2.54 for **2-NP**. We observed a reduction in the breakthrough time and the lower pressures at the inlet of the column with **2-box**, compared with **2-NP** (the inlet pressure = 19.2 and 50.3 kPa; hexane breakthrough time = 6.8 and 9.9 min; 2,2-dimethylbutane breakthrough time = 1.9 and 3.3 min for the **2-box** and **2-NP**, respectively). As seen in TEM image of **2-box** sliced by a microtome (Figure 2d), the epoxy resin penetrated into the inside of **2-box** in spite of its bulkiness, suggesting that the molecules can easily pass through the grain boundaries of nanocrystals into the internal voids of **2-box**. The interior voids of **2-box** provides the paths for the hydrocarbons to diffuse faster in the column, leading to the shorter separation time and lower inlet pressure. These results show that the box superstructure enables the quick separation while keeping separation efficiency.

## CONCLUSION

We have integrated the bidirectional diffusion of multiple components into molecular assembly, which gives the box superstructure of a solid-solution PCP. The reaction of crystals of  $[\text{Zn}_2(\text{ndc})_2(\text{bpy})]_n$  with  $\text{H}_2\text{bdc}$  was carried out. The dissolution of the parent crystals generates the outward diffusion of components ( $\text{Zn}^{2+}$  and  $\text{bpy}$ ), and contrariwise, the other dicarboxylate of  $\text{bdc}$  is accumulated on the surface of the parent crystals. This bidirectional diffusion of components spatially localized the recrystallization of solid-solution PCP at the surface of the parent cuboid crystals; therefore, the nanocrystals of solid-solution PCP,  $[\text{Zn}_2(\text{bdc})_{1.5}(\text{ndc})_{0.5}(\text{bpy})]_n$ , were organized into the box superstructure. The box superstructure enhanced the mass transfer kinetics for the molecular separation. We believe that this work provides a new strategy to fabricate the smart porous materials in which properties of PCP itself and macroscopic morphology are synergistically integrated.

## EXPERIMENTAL SECTION

**Synthesis of the Single Crystals, 1.**  $\text{Zn}(\text{NO}_3)_2 \cdot 6\text{H}_2\text{O}$  (72.3 mg,  $2.5 \times 10^{-1}$  mmol), 1,4-naphthalenedicarboxylic acid (54.0 mg,  $2.5 \times 10^{-1}$  mmol) and 4,4'-bipyridyl (21.0 mg,  $1.25 \times 10^{-1}$  mmol) were dissolved in 5 mL of *N,N*-dimethylformamide (DMF). The temperature was kept at 80 °C for 2 days. After cooling, single crystals were harvested.

**Synthesis of the Powder Crystals, 1.**  $\text{Zn}(\text{NO}_3)_2 \cdot 6\text{H}_2\text{O}$  (148.5 mg,  $5.0 \times 10^{-1}$  mmol), 1,4-naphthalenedicarboxylic acid (108.0 mg,  $5.0 \times 10^{-1}$  mmol) and 4,4'-bipyridyl (42.0 mg,  $2.5 \times 10^{-1}$  mmol) were dissolved in 10 mL of DMF. The temperature was kept at 120 °C for 3 h by microwave instrument (Biotage, Initiator).

**Synthesis of 2-box.** 1,4-Benzenedicarboxylic acid (16.6 mg,  $1.0 \times 10^{-1}$  mmol) was dissolved in 2 mL of DMF. The powder crystals of **1** (8.0 mg,  $2.0 \times 10^{-2}$  mmol) were placed in the solution, and the temperature was kept at 80 °C by a microwave reactor (Biotage, Initiator).

**Synthesis of 2-box in Millimeter Scale.**  $\text{Zn}(\text{NO}_3)_2 \cdot 6\text{H}_2\text{O}$  (5.94 mg,  $2.0 \times 10^{-2}$  mmol), 1,4-benzenedicarboxylic acid (3.32 mg,  $2.0 \times 10^{-2}$  mmol) and 4,4'-bipyridyl (1.68 mg,  $1.0 \times 10^{-2}$  mmol) were dissolved in 1 mL of DMF. A single crystal of **1** with the millimeter scale was placed in the stocked solution, and the temperature was kept at 120 °C for 2 days. After cooling, the **2-box** with the millimeter scale was obtained.

**Synthesis of 2-micro.**  $\text{Zn}(\text{NO}_3)_2 \cdot 6\text{H}_2\text{O}$  (11.9 mg,  $4.0 \times 10^{-2}$  mmol),  $\text{H}_2\text{bdc}$  (5.3 mg,  $3.2 \times 10^{-2}$  mmol), and  $\text{H}_2\text{ndc}$  (1.7 mg,  $0.8 \times 10^{-2}$  mmol) were dissolved in 2 mL of DMF. 4,4'-bipyridyl (1.6 mg,  $1.0 \times 10^{-2}$  mmol) was dissolved in 1 mL of methanol. 2 mL of DMF solution, 0.5 mL of the buffer mixture of DMF/methanol (1:1) and 1 mL of methanol solution was sequentially layered from bottom to top in a narrow glass tube. The stocked solution was kept at 90 °C for 2 days. A largest crystal (10  $\mu\text{m}$ ) was picked up for the single-crystal X-ray structure analysis.

**Decomposition of 2-box.** The ultrasonication of dozens of **2-box** in DMF was carried out for 10 min. The box superstructures were completely decomposed.

**$^1\text{H}$  NMR on Digested 2-box.** The dozens of crystals are decomposed in dimethyl sulfoxide- $d_6$  with hydrochloric acid. The obtained solution was analyzed by 500 MHz  $^1\text{H}$  NMR (JNM-AS00).

**$^1\text{H}$  NMR on Residual Solution.** The mixture of 0.3 mL of the residual solution, 0.3 mL of dimethyl sulfoxide- $d_6$  and 40.6  $\mu\text{L}$  of methanol was analyzed by 500 MHz  $^1\text{H}$  NMR (JNM-AS00). The peaks of  $\text{H}_2\text{bdc}$ ,  $\text{H}_2\text{ndc}$  and methanol were fitted by Lorentz function to calculate the integration areas of peaks.

**Field-Emission Scanning Electron Microscopy (FE-SEM).** SEM observations were performed with a JEOL Model JSM-7001F4 SEM system operating at 15.0 kV. The samples were deposited on carbon tape and coated with osmium prior to the measurement.

**Ultrathin Section Transmission Electron Microscopy (TEM).** Dozens of dried **2-boxes** were immersed in thermoset epoxy resin (EPON 812/TAAB Laboratories Equipment Ltd., UK) and heated at 65 °C for few days. The solidified sample was sliced by ultramicrotome (Leica FC6, AU). The ultrathin sections ( $\sim 60$  nm) were mounted on EM grids and then observed by TEM (JEOL JEM1400, Japan).

**X-ray Diffraction (XRD) and Surface X-ray Diffraction (SXRD) Measurements.** The samples were deposited on glass substrates. XRD and SXRD patterns were recorded by RINT-2000 (Rigaku) and Smart Lab (Rigaku), respectively.

**Synthesis of Box Superstructure of IR-MOF.** 2-Aminobenzene-1,4-dicarboxylic acid (18.1 mg, 0.1 mmol) was dissolved in the mixture of DMF and ethanol (2 mL, DMF: ethanol = 1:1). The microcrystals of MOF-5 (5.0 mg), synthesized according to literature procedures,<sup>29b</sup> were placed into the solution, and the temperature was kept at 60 °C for 2 h by microwave reactor.

**Sorption Experiments.** The sorption isotherms of **1** and the **2-box** for nitrogen, oxygen and carbon dioxide were recorded on a BELSORP-mini adsorption instrument from BEL Japan, Inc. Prior to the adsorption measurements, the samples were evacuated under vacuum at 323 K for 6 h.

**Sorption Kinetics.** The sorption kinetics of 2-micro and 2-box for carbon dioxide and *n*-hexane were recorded on a BELSORP-18 adsorption instrument from BEL Japan, Inc. The pressure value of the sample tube was recorded every 1 second. Prior to the adsorption measurements, the samples were degassed under vacuum at 323 K for 6 h.

**Breakthrough Measurements in Vapor Phase.** Breakthrough experiments in vapor phase for the equimolar hexane/2,2-dimethylbutane gas mixture were performed using the experimental setup described in Figure S36. Briefly, 0.09 g of the 2-box and the 2-NP were packed in a glass tube ( $L = 5$  cm; diameter = 3 mm) by helium gas pressure (1.69 Pa  $m^3/s$ ). The adsorption column was then placed in an oven at 40 °C and operated by introducing continuously a hexane/2,2-dimethylbutane vapor mixture generated by BELFlow-3 from BEL JAPAN. The composition history of the mixtures collected at the outlet of the column was evaluated by a gas chromatographer GC-2014 from SHIMADZU. A flame ionization detector was connected to the GC column outlet.

**Structure Determination.** X-ray data collection ( $5^\circ < 2\theta < 55^\circ$ ) was conducted at 223 K on Rigaku AFC10 diffractometer Mo  $K\alpha$  radiation ( $\lambda = 0.7105$  Å) with Rigaku Mercury CCD system. The structures were solved by a direct method (SIR2002) and expanded using Fourier techniques. All calculations were performed using the CrystalStructure crystallographic software package 4.0 of Rigaku. The data can be obtained free of charge from The Cambridge Crystallographic Data Centre via [www.ccdc.cam.ac.uk/data\\_request/cif](http://www.ccdc.cam.ac.uk/data_request/cif).

**Crystal Data for 1**  $\supset$  Solvent.  $C_{34}H_{20}N_2O_8Zn_2$ , tetragonal, space group  $P4/mmm$ , (no. 123),  $a = 10.9396(6)$  Å,  $c = 14.0640(11)$  Å,  $V = 1683.11(19)$  Å<sup>3</sup>,  $Z = 1$ ,  $T = 223$  K.  $\rho_{\text{calcd}} = 1.148$  g  $cm^{-3}$ ,  $\mu(\text{Mo } K\alpha) = 0.776$   $cm^{-1}$ , 1185 reflections measured, 985 observed ( $I > 2.00\sigma(I)$ ) 63 parameters;  $R_1 = 0.0692$ ,  $wR_2 = 0.2315$ , GOF = 1.158. Elemental analysis calcd. for  $C_{43}H_{45}N_5O_8Zn_2 \{ [Zn_2(\text{ndc})_2(\text{bpy})] \cdot (\text{DMF})_4(\text{H}_2\text{O})_3 \}_n$ : C, 52.04; H, 5.13; N, 7.92. Found: C, 49.82; H, 4.90; N, 7.99. The hydrogens and solvent molecules are severely disordered. The atom of C5 has high ADP max/min ratio because of the rotation of the pyridyl ring. (CCDC: 1017400)

**Crystal Data for 2**  $\supset$  Solvent.  $C_{31}H_{21}N_3O_9Zn_2$ , triclinic, space group  $P\bar{1}$ , (no. 2),  $a = 10.887(3)$  Å,  $b = 10.923(3)$  Å,  $c = 14.068(4)$  Å,  $\alpha = 89.214(8)^\circ$ ,  $\beta = 87.590(7)^\circ$ ,  $\gamma = 79.816(8)^\circ$ ,  $V = 1645.1(7)$  Å<sup>3</sup>,  $Z = 2$ ,  $T = 93$  K.  $\rho_{\text{calcd}} = 1.434$  g  $cm^{-3}$ ,  $\mu(\text{Mo } K\alpha) = 1.513$   $cm^{-1}$ , 13134 reflections measured, 7178 observed ( $I > 2.00\sigma(I)$ ) 446 parameters;  $R_1 = 0.0512$ ,  $wR_2 = 0.1835$ , GOF = 1.098. Elemental analysis calcd. for  $C_{34}H_{35}N_4O_{12}Zn_2 \{ [Zn_2(\text{ndc})_{1.5}(\text{ndc})_{0.5}(\text{bpy})] \cdot (\text{DMF})_2(\text{H}_2\text{O})_2 \}_n$ : C, 49.65; H, 4.29; N, 6.81. Found: C, 49.37; H, 3.46; N, 5.56. The hydrogens are severely disordered. The atoms of C12 and C18 cannot be refined anisotropically, because C12 and C18 are located very close to C11 and C17, respectively (bdc and ndc are located in the same site in 50% each). The atoms of C15, C29, C30 and C31 has high ADP max/min ratio because of the rotation of the pyridyl ring and benzene ring. (CCDC: 1017401)

**Crystal Data for 2.**  $C_{56}H_{34}N_4O_{16}Zn_4$ , orthorhombic, space group  $Cmme$ , (no. 67),  $a = 9.923(16)$  Å,  $b = 19.10(3)$  Å,  $c = 14.33(3)$  Å,  $V = 2715(8)$  Å<sup>3</sup>,  $Z = 2$ ,  $T = 93$  K.  $\rho_{\text{calcd}} = 1.600$  g  $cm^{-3}$ ,  $\mu(\text{Mo } K\alpha) = 1.859$   $cm^{-1}$ , 20578 reflections measured, 1669 observed ( $I > 2.00\sigma(I)$ ) 162 parameters;  $R_1 = 0.1428$ ,  $wR_2 = 0.13874$ , GOF = 1.333. Elemental analysis calcd. for  $C_{28}H_{17}N_2O_8Zn_2 \{ [Zn_2(\text{ndc})_{1.5}(\text{ndc})_{0.5}(\text{bpy})] \}_n$ : C, 52.53; H, 2.68; N, 4.38. Found: C, 51.37; H, 2.59; N, 4.16. The hydrogens are severely disordered. (CCDC: 1017402).

## ■ ASSOCIATED CONTENT

### Supporting Information

Experimental details, XRD, <sup>1</sup>H NMR, surface XRD, single crystal structure, gas adsorption isotherms, thermogravimetric analysis, SEM, fitting analyses of sorption kinetics and breakthrough measurement, and CIF files. This material is available free of charge via the Internet at <http://pubs.acs.org>.

## ■ AUTHOR INFORMATION

### Corresponding Authors

shuhei.furukawa@icems.kyoto-u.ac.jp

kitagawa@icems.kyoto-u.ac.jp

### Notes

The authors declare no competing financial interest.

## ■ ACKNOWLEDGMENTS

K. H. is grateful to JSPS Research Fellowships for Young Scientists. The authors thank Chiwon Kim (Kyoto University) for his assistance for the experiments. iCeMS is supported by World Premier International Research Initiative (WPI), MEXT, Japan. The authors thank EM facility/CeMI for assistance with electron microscopy.

## ■ REFERENCES

- (1) Swiegers, G. F.; Malefsetse, T. J. *Chem. Rev.* **2000**, *100*, 3483–3537.
- (2) Whitesides, G. M.; Grzybowski, B. *Science* **2002**, *295*, 2418–2421.
- (3) Lehn, J. M. *Science* **2002**, *295*, 2400–2403.
- (4) Hirschberg, J. H. K. K.; Brunsveld, L.; Ramzi, A.; Vekemans, J. A. J. M.; Sijbesma, R. P.; Meijer, E. W. *Nature* **2000**, *407*, 167–170.
- (5) Fujita, M. *Chem. Soc. Rev.* **1998**, *27*, 417–425.
- (6) Caplan, M. R.; Moore, P. N.; Zhang, S. G.; Kamm, R. D.; Lauffenburger, D. A. *Biomacromolecules* **2000**, *1*, 627–631.
- (7) (a) Yin, Y. D.; Rioux, R. M.; Erdonmez, C. K.; Hughes, S.; Somorjai, G. A.; Alivisatos, A. P. *Science* **2004**, *304*, 711–714. (b) Wesson, P. J.; Soh, S.; Klajn, R.; Bishop, K. J. M.; Gray, T. P.; Grzybowski, B. A. *Adv. Mater.* **2009**, *21*, 1911–1915.
- (8) (a) Yaghi, O. M.; O’Keeffe, M.; Ockwig, N. W.; Chae, H. K.; Eddaoudi, M.; Kim, J. *Nature* **2003**, *423*, 705–714. (b) Kitagawa, S.; Kitaura, R.; Noro, S. *Angew. Chem., Int. Ed.* **2004**, *43*, 2334–2375. (c) Ferey, G.; Serre, C. *Chem. Soc. Rev.* **2009**, *38*, 1380–1399. (d) Murray, L. J.; Dincă, M.; Long, J. R. *Chem. Soc. Rev.* **2009**, *38*, 1294–1314. (e) Batten, S. R.; Robson, R. *Angew. Chem., Int. Ed.* **1998**, *37*, 1460–1494.
- (9) (a) Vaidhyanathan, R.; Iremonger, S. S.; Shimizu, G. K. H.; Boyd, P. G.; Alavi, S.; Woo, T. K. *Science* **2010**, *330*, 650–653. (b) Rabone, J.; Yue, Y. F.; Chong, S. Y.; Stylianou, K. C.; Bacsa, J.; Bradshaw, D.; Darling, G. R.; Berry, N. G.; Khimyak, Y. Z.; Ganin, A. Y.; Wiper, P.; Claridge, J. B.; Rosseinsky, M. J. *Science* **2010**, *329*, 1053–1057.
- (10) (a) Farha, O. K.; Malliakas, C. D.; Kanatzidis, M. G.; Hupp, J. T. *J. Am. Chem. Soc.* **2010**, *132*, 950–952. (b) Li, J. R.; Zhou, H. C. *Nat. Chem.* **2010**, *2*, 893–898. (c) Ma, L. Q.; Lin, W. B. *J. Am. Chem. Soc.* **2008**, *130*, 13834–13835. (d) Mohideen, M. I. H.; Xiao, B.; Wheatley, P. S.; McKinlay, A. C.; Li, Y.; Slawin, A. M. Z.; Aldous, D. W.; Cessford, N. F.; Duren, T.; Zhao, X. B.; Gill, R.; Thomas, K. M.; Griffin, J. M.; Ashbrook, S. E.; Morris, R. E. *Nat. Chem.* **2011**, *3*, 304–310.
- (11) (s) Ma, S.; Sun, D.; Simmons, J. M.; Collier, C. D.; Yuan, D.; Zhou, H. C. *J. Am. Chem. Soc.* **2008**, *130*, 1012–1016. (b) Dincă, M.; Dailly, A.; Liu, Y.; Brown, C. M.; Neumann, D. A.; Long, J. R. *J. Am. Chem. Soc.* **2006**, *128*, 16876–16883. (c) Matsuda, R.; Kitaura, R.; Kitagawa, S.; Kubota, Y.; Belosludov, R. V.; Kobayashi, T. C.; Sakamoto, H.; Chiba, T.; Takata, M.; Kawazoe, Y.; Mita, Y. *Nature* **2005**, *436*, 238–241.
- (12) (a) Wang, B.; Côté, A. P.; Furukawa, H.; O’Keeffe, M.; Yaghi, O. M. *Nature* **2008**, *453*, 207–211. (b) Alaerts, L.; Kirschhock, C. E. A.; Maes, M.; van der Veen, M. A.; Finsy, V.; Depla, A.; Martens, J. A.; Baron, G. V.; Jacobs, P. A.; Denayer, J. F. M.; De Vos, D. E. *Angew. Chem., Int. Ed.* **2007**, *46*, 4293–4297.
- (13) (a) Wu, C.-D.; Hu, A.; Zhang, L.; Lin, W. *J. Am. Chem. Soc.* **2005**, *127*, 8940–8941. (b) Corma, A.; Garcia, H.; Llabres i Xamena, F. X. *Chem. Rev.* **2010**, *110*, 4606–4655.
- (14) (a) Fukushima, T.; Horike, S.; Inubushi, Y.; Nakagawa, K.; Kubota, Y.; Takata, M.; Kitagawa, S. *Angew. Chem., Int. Ed.* **2010**, *49*, 4820–4824. (b) Deng, H. X.; Doonan, C. J.; Furukawa, H.; Ferreira, R. B.; Towne, J.; Knobler, C. B.; Wang, B.; Yaghi, O. M. *Science* **2010**, *327*, 846–850. (c) Fukushima, T.; Horike, S.; Kobayashi, H.; Tsujimoto, M.;

- Isoda, S.; Foo, M. L.; Kubota, Y.; Takata, M.; Kitagawa, S. *J. Am. Chem. Soc.* **2012**, *134*, 13341–13347. (d) Horike, S.; Inubushi, Y.; Hori, T.; Fukushima, T.; Kitagawa, S. *Chem. Sci.* **2012**, *3*, 116–120. (e) Kong, X.; Deng, H.; Yan, F.; Kim, J.; Swisher, J. A.; Smit, B.; Yaghi, O. M.; Reimer, J. A. *Science* **2013**, *341*, 882–885.
- (15) Furukawa, S.; Reboul, J.; Diring, S.; Sumida, K.; Kitagawa, S. *Chem. Soc. Rev.* **2014**, *43*, 5700–5734.
- (16) (a) Hermes, S.; Schroder, F.; Chelmoski, R.; Wöll, C.; Fischer, R. A. *J. Am. Chem. Soc.* **2005**, *127*, 13774–13745. (b) Shekhah, O.; Wang, H.; Kowarik, S.; Schreiber, F.; Paulus, M.; Tolan, M.; Sternemann, C.; Evers, F.; Zacher, D.; Fischer, R. A.; Wöll, C. *J. Am. Chem. Soc.* **2007**, *129*, 15118–15119. (c) Biemmi, E.; Scherb, C.; Bein, T. *J. Am. Chem. Soc.* **2007**, *129*, 8054–8055. (d) Tsotsalas, M.; Umemura, A.; Kim, F.; Sakata, Y.; Reboul, J.; Kitagawa, S.; Furukawa, S. *J. Mater. Chem.* **2012**, *22*, 10159–10165. (e) Makiura, R.; Motoyama, S.; Umemura, Y.; Yamanaka, H.; Sakata, O.; Kitagawa, H. *Nat. Mater.* **2010**, *9*, 565–571. (f) Lia, M.; Dincă, M. *Chem. Sci.* **2014**, *5*, 107–111. (g) Bradshaw, D.; Garai, A.; Huo, J. *Chem. Soc. Rev.* **2012**, *41*, 2344–2381.
- (17) (a) Falcaro, P.; Hill, A. J.; Nairn, K. M.; Jasieniak, J.; Mardel, J. I.; Bastow, T. J.; Mayo, S. C.; Gimona, M.; Gomez, D.; Whitfield, H. J.; Ricco, R.; Patelli, A.; Marmiroli, B.; Amenitsch, H.; Colson, T.; Villanova, L.; Buso, D. *Nat. Commun.* **2011**, *2*, 237. (b) Reboul, J.; Furukawa, S.; Horike, N.; Tsotsalas, M.; Hirai, K.; Uehara, H.; Kondo, M.; Louvain, N.; Sakata, O.; Kitagawa, S. *Nat. Mater.* **2012**, *11*, 717–723. (c) Doherty, C. M.; Greci, G.; Riccò, R.; Mardel, J. I.; Reboul, J.; Furukawa, S.; Kitagawa, S.; Hill, A. J.; Falcaro, P. *Adv. Mater.* **2013**, *25*, 4701–4705.
- (18) (a) Ameloot, R.; Vermoortele, F.; Vanhove, W.; Roeffaers, M. B. J.; Sels, B. F.; De Vos, D. E. *Nat. Chem.* **2011**, *3*, 382–387. (b) Carne-Sanchez, A.; Imaz, I.; Cano-Sarabia, M.; MasPOCH, D. *Nat. Chem. Biol.* **2013**, *5*, 203–211. (c) Kuo, C. H.; Tang, Y.; Chou, L. Y.; Sneed, B. T.; Brodsky, C. N.; Zhao, Z. P.; Tsung, C. K. *J. Am. Chem. Soc.* **2012**, *134*, 14345–14348. (d) Li, A. L.; Ke, F.; Qiu, L. G.; Jiang, X.; Wang, Y. M.; Tian, X. Y. *CrystEngComm* **2013**, *15*, 3554–3559.
- (19) (a) Furukawa, S.; Hirai, K.; Nakagawa, K.; Takashima, Y.; Matsuda, R.; Tsuruoka, T.; Kondo, M.; Haruki, R.; Tanaka, D.; Sakamoto, H.; Shimomura, S.; Sakata, O.; Kitagawa, S. *Angew. Chem., Int. Ed.* **2009**, *48*, 1766–1779. (b) Koh, K.; Wong-Foy, A. G.; Matzger, A. J. *Chem. Commun.* **2009**, 6162–6164. (c) Hirai, K.; Furukawa, S.; Kondo, M.; Uehara, H.; Sakata, O.; Kitagawa, S. *Angew. Chem., Int. Ed.* **2011**, *50*, 8057–8061. (d) Li, T.; Sullivan, J. E.; Rosi, N. L. *J. Am. Chem. Soc.* **2013**, *135*, 9984–9987.
- (20) (a) Wu, Y.; Li, F.; Zhu, W.; Cui, J.; Tao, C.; Lin, C.; Hannam, P. M.; Li, G. *Angew. Chem., Int. Ed.* **2011**, *50*, 12518–12522. (b) Schoedel, A.; Scherb, C.; Bein, T. *Angew. Chem., Int. Ed.* **2010**, *49*, 7225–7228.
- (21) (a) Khaletskaya, K.; Reboul, J.; Meilikhov, M.; Nakahama, M.; Diring, S.; Tsujimoto, M.; Isoda, S.; Kim, F.; Kamei, K.; Fischer, R. A.; Kitagawa, S.; Furukawa, S. *J. Am. Chem. Soc.* **2013**, *135*, 10998–11005. (b) Zhan, W.; Kuang, Q.; Zhou, J.; Kong, X.; Xie, Z.; Zhen, L. *J. Am. Chem. Soc.* **2013**, *135*, 1926–1933.
- (22) Kambe, T.; Sakamoto, R.; Hoshiko, K.; Takada, K.; Miyachi, M.; Ryu, J.; Sasaki, S.; Kim, J.; Nakazato, K.; Takata, M.; Nishihara, H. *J. Am. Chem. Soc.* **2013**, *135*, 2462–2465.
- (23) (a) Seki, K.; Mori, W. *J. Phys. Chem. B* **2002**, *106*, 1380–1385. (b) Dybtsev, D. N.; Chun, H.; Kim, K. *Angew. Chem., Int. Ed.* **2004**, *43*, 5033–5036. (c) Ma, B. Q.; Mulfort, K. L.; Hupp, J. T. *Inorg. Chem.* **2005**, *44*, 4912–4914. (d) Chen, B.; Liang, C. D.; Yang, J.; Contreras, D. S.; Clancy, Y. L.; Lobkovsky, E. B.; Yaghi, O. M.; Dai, S. *Angew. Chem., Int. Ed.* **2006**, *45*, 1390–1393.
- (24) (a) Henke, S.; Schneemann, A.; Wütscher, A.; Fischer, R. A. *J. Am. Chem. Soc.* **2012**, *134*, 9464–9474. (b) Kozachuk, O.; Khaletskaya, K.; Halbherr, M.; Bétard, A.; Meilikhov, M.; W. Seidel, R.; Jee, B.; Pöppel, A.; Fischer, R. A. *Eur. J. Inorg. Chem.* **2012**, 1688–1695.
- (25) Hirai, K.; Chen, K.; Fukushima, T.; Horike, S.; Kondo, M.; Louvain, N.; Kim, C.; Sakata, Y.; Meilikhov, M.; Sakata, O.; Kitagawa, S.; Furukawa, S. *Dalton Trans.* **2013**, *42*, 15868–15872.
- (26) (a) Shekhah, O.; Wang, H.; Zacher, D.; Fischer, R. A.; Wöll, C. *Angew. Chem., Int. Ed.* **2009**, *48*, 5038–5041. (b) Scherb, C.; Schödel, A.; Bein, T. *Angew. Chem., Int. Ed.* **2008**, *47*, 5777–5779.
- (27) Qiao, Z. A.; Chai, S. H.; Nelson, K.; Bi, Z.; Chen, J.; Mahurin, M. S.; Zhu, X.; Dai, S. *Nat. Commun.* **2014**, *5*, 3705.
- (28) Fan, H. J.; Gösele, U.; Zacharias, M. *Small* **2007**, *3*, 1660–1671.
- (29) (a) Eddaoudi, M.; Kim, J.; Rosi, N.; Vodak, D.; Wachter, J.; O’Keeffe, M.; Yaghi, O. M. *Science* **2002**, *295*, 469–472. (b) Tranchemontagne, D. J.; Hunt, J. R.; Yaghi, O. M. *Tetrahedron* **2008**, *64*, 8553–8557.
- (30) (a) Dincă, M.; Dailly, A.; Tsay, C.; Long, J. R. *Inorg. Chem.* **2008**, *47*, 11–13. (b) Jiang, H. L.; Makala, T. A.; Zhou, H. C. *Coord. Chem. Rev.* **2013**, *257*, 2232–2249.
- (31) (a) Fletcher, A. J.; Cussen, E. J.; Bradshaw, D.; Rosseinsky, M. J.; Thomas, K. M. *J. Am. Chem. Soc.* **2004**, *126*, 9750–9759. (b) Chen, B.; Zhao, X.; Putkham, A.; Hong, K.; Lobkovsky, E. B.; Hurtado, E. J.; Fletcher, A. J.; Thomas, K. M. *J. Am. Chem. Soc.* **2008**, *130*, 6411–6423.
- (32) Rao, M. B.; Jenkins, R. G.; Steele, W. A. *Langmuir* **1985**, *1*, 137–139.
- (33) (a) Barcia, P. S.; Zapata, F.; Silva, J. A. C.; Rodrigues, A. E.; Chen, B. *J. Phys. Chem. B* **2007**, *111*, 6101–6103. (b) Nakagawa, K.; Tanaka, D.; Horike, S.; Shimomura, S.; Higuchia, M.; Kitagawa, S. *Chem. Commun.* **2010**, *46*, 4258–4260. (c) Bux, H.; Liang, F. Y.; Li, Y. S.; Cravillon, J.; Wiebecke, M.; Caro, J. *J. Am. Chem. Soc.* **2009**, *131*, 16000–16001. (d) Ferreira, A. F. P.; Mittelmeijer-Hazeleger, M. C.; Granato, M. A.; Martins, V. F. D.; Rodrigues, A. E.; Rothenberg, G. *Phys. Chem. Chem. Phys.* **2013**, *15*, 8795–8804. (e) Han, S. B.; Wei, Y. H.; Valente, C.; Lagzi, I.; Gassensmith, J. J.; Coskun, A.; Stoddart, J. F.; Grzybowski, B. A. *J. Am. Chem. Soc.* **2010**, *132*, 16358–16361.